Journal of Electroanalytical Chemistry 837 (2019) 30–38

Contents lists available at ScienceDirect

Journal of Electroanalytical Chemistry

journal homepage: www.elsevier.com/locate/jelechem

# Green, single-pot synthesis of functionalized Na/N/P co-doped graphene nanosheets for high-performance supercapacitors

Dalia M. El-Gendy[a,b], Nabil A. Abdel Ghany[a,*], Nageh K. Allam[b,*]

[a] Physical Chemistry Department, National Research Centre, Dokki, Giza, Egypt
[b] Energy Materials Laboratory (EML), School of Sciences and Engineering, The American University in Cairo, New Cairo 11835, Egypt

ARTICLE INFO

*Keywords:*
Supercapacitors
Graphene
Doping
Cycling retention
Capacitance
Green synthesis

ABSTRACT

The synthesis of heteroatom-doped graphene nanosheets is one of the recent trends to improve the energy storage capabilities of graphene in devices such as supercapacitors. We report on the optimized fabrication of sodium-nitrogen-phosphorus co-doped graphene sheets (Na/N/P-GNS) via a simple one-pot green method. The fabricated Na/N/P-GNS were characterized using X-ray diffraction (XRD), Raman spectroscopy, thermogravimetric analysis (TGA), FTIR, scanning electron microscopy (FESEM), X-ray photoelectron spectroscopy (XPS), and transmission electron microscopy (TEM). Various electrochemical techniques were used to investigate the capacitance and performance of the prepared Na/N/P-GNS, including cyclic voltammetry (CV) at different potential scan rates and electrochemical charge/discharge at different current densities in 0.5 M $H_2SO_4$ aqueous electrolyte at room temperature. Na/N/P-GNS showed a maximum specific capacitance of 499 F/g at a scan rate of 1 mV/s, excellent cycling retention of 101% after 1000 cycles at 200 mV/s, and high energy density of 98.58 $Whkg^{-1}$. The high capacitance can be ascribed to the co-doping of Na, P and N and the one-pot synthesis methods that retain the graphene sheets unstacked. Based on the obtained capacitance, the fabricated Na/N/P-GNS would be a promising electrode material for supercapacitors.

## 1. Introduction

Electrochemical supercapacitors have gained much attention recently due to their high power density, reversibility, lengthy life cycle, and their environmentally friendly nature [1]. According to the type of materials and reaction mechanisms involved, supercapacitors are divided into three types: electrical double layer capacitors (EDLCs), Faradic pseudocapacitors, and hybrid supercapacitors [2]. EDLCs store their energy physically by the adsorption of charge growth on the electrode/electrolyte interface, resulting in an increase in the power density and cycle life compared to secondary batteries [3]. Pseudocapacitors (battery type) store energies chemically due to the reversible Faradic reactions on the electrode material [4]. The pseudocapacitive materials, such as transition metal oxides and conducting polymers [5,6], can attain reasonably higher capacitance than EDLCs but are narrow by the poor cyclability as the involved redox reactions lead to structural decay of the electrode material [7]. Therefore, many efforts have been ardent to improve the energy density of EDLCs by integrating EDLCs materials with pseudocapacitive materials to form hybrid electrochemical supercapacitors [8–11]. In this regard, many carbon-based materials, such as carbon nanotubes, activated carbons (AC), graphite, graphene oxide (GO) and graphene, have been actively investigated due to their availability, ease of preparation, and varied temperature range [12,13]. Of special interest, graphene is given much attention as an active electrode material due to its distinctive properties, including excellent electrical and mechanical properties, chemical stability, high specific surface area, and the viability for large-scale chemical fabrication of modified graphene [14–16]. The synthesis of graphene by chemical reduction is one of the most public methods to prepare graphene using reducing reagents such as hydrazine, dimethyl hydrazine, and sodium borohydrate [17–20]. However, they are unsafe to the environment and create strong graphene propensity to restack due to the π–π contacts [17–20]. To this end, doping graphene with heteroatoms is introduced as a solution to prevent the restacking of the sheets [21]. For example, N-doped graphene was developed using multiple techniques such chemical vapor deposition (CVD) using $CH_4$ in existence of $NH_3$ [22], current arc discharge between graphite electrodes with $NH_3$ and pyridine vapor [23], thermal expansion of graphite oxides in the presence of $N_2$ plasma [24], electrothermal reactions with ammonia [25], annealing of graphene with ammonia at 900 °C [26], plasma treatment of graphene synthesized via a chemical method [27], and expanded graphite in the presence of acetonitrile at 310 °C [28].

* Corresponding authors.
*E-mail addresses:* na_manakhly@yahoo.co.uk (N.A. Abdel Ghany), nageh.allam@aucegypt.edu (N.K. Allam).

https://doi.org/10.1016/j.jelechem.2019.02.009
Received 31 January 2019; Received in revised form 7 February 2019; Accepted 7 February 2019
Available online 08 February 2019

Also, P-doped graphite layers were synthesized via the pyrolysis of toluene with triphenyl phosphine [29] or annealing a mixture of graphene oxide in the presence of an ionic liquid such as 1-butyl-3-methlyimidazolium hexafluoro phosphate [30]. Further, B-and N-doped graphene was synthesized via the gas phase arc discharge in the presence of a B/N sources [31]. However, those methods use toxic reagents, require the use of specific set-ups, reducing gasses, and higher temperatures for longer periods of time [32]. Therefore, it is necessary to develop synthesis protocols that use environmentally friendly materials and nontoxic reducing reagent (green agents) that are able to perform the reduction process while preventing the aggregation of the reduced graphene oxide sheets via doping of such sheets with heteroatoms.

Herein, we present a very simple, on-pot and green method for the synthesis of Na/N/P co-doped graphene sheets via the reaction of spongy graphene oxide (SGO) in the existence of guanosine monophosphate as a green reagent and investigating its performance as a supercapacitors material. Our rational behind the use of P is that it is a more electron-rich atom compared to carbon and can be easily doped into the graphene basal plane to modify the chemical properties of graphene. Also, P has larger atomic radius and greater electron donating properties than N, suggesting its potential to enhance the catalytic properties of graphene in electrochemical devices [33].

## 2. Experimental methods and materials

### 2.1. Materials

"Graphite powder (< 20 μm, Sigma Aldrich), Nafion® 117 solution (5%, Sigma Aldrich), sulfuric acid ($H_2SO_4$ 99%, Sham lab), hydrogen peroxide ($H_2O_2$ 30% W/V, LOBA Chemie), absolute ethanol (El-Nasr pharmaceutical company, Egypt), HCl (33%, El-Nasr pharmaceutical company, Egypt), potassium permanganate ($KMnO_4$99%, Arabic Laboratory Equipment Co.), and guanosine monophosphate disodium salt (Merk) were used directly without further purification. Distillated water was used for washing the products.

### 2.2. Synthesis of spongy graphene oxide (SGO)

Graphene oxide (GO) was prepared from natural graphite using a modified Hummers method [34]. In a typical experiment, graphite (1.5 g), $NaNO_3$ (1.5 g) and $H_2SO_4$ (70 ml) were mixed and stirred in an ice bath. Subsequently, 9 g of $KMnO_4$were added slowly. The reaction mixture was warmed to 40 °C and stirred for 1 h. Water (100 ml) was then added and the temperature was increased to 90 °C for 30 min. Finally, 300 ml of water were added slowly, followed by the slow addition of 10 ml of 30% $H_2O_2$. The reaction mixture was filtered and washed with 0.1 M HCl and water. The GO precipitate was dispersed in a water/methanol (1:5) mixture and purified by three repeated centrifugation steps at 10000 rpm for 30 min. The purified sample was dispersed in deionized water and centrifuged at 2500 rpm and finally washed by deionized water and sonicatedfor1 hour to obtain highly exfoliated GO. Then, the obtained GO was dispersed in water/Methanol mixture and purified with repeated centrifugation steps at 10000 rpm for 30 min, washed with 0.1 M of HCl and water to obtain highly exfoliated GO sheets. To prepare SGO, GO solution (4 mg/1 ml) in a tube was frozen by place the tube in a freezer at a freezing temperature of-18 °C for 2 days. After the GO solution was completely frozen, the tube was peregrinated to a freeze-dryer and dried at a temperature of −53 °C and a pressure of 10pa for 3 days to finally obtain the SGO [35].

### 2.3. Synthesis of covalently functionalized graphene with guanosine monophosphate disodium salt

Go (0.1 g) was dispersed in distilled water (10 ml) and then (0.3 g) guanosine monophosphate and an equimolar amount of NaOH in distilled water(10 ml) were added. The mixture was stirred for 24 h toprecipitate, which was then centrifuged, washed with water/ethanol mixture and at the end dried at 60 °C [36] (Scheme 1).

### 2.4. Preparation of electrodes and electrochemical measurements

"Glassy carbon (GC) electrode (5.0 mm diameter) was polished with alumina nanopowder and rinsed with deionized water. Fresh dispersion of the sample was prepared for each experiment by dispersing 5.0 mg of each sample in 0.5 ml Nafion® 117 solution (1%) by ultrasonication for 30 min. Then, 10 μl suspension of the material was casted onto the surface of the electrode with a micropipette. Finally, the working electrode was dried at 60 °C for 10 min and left to cool down. All the electrochemical measurements were performed in a three-electrode

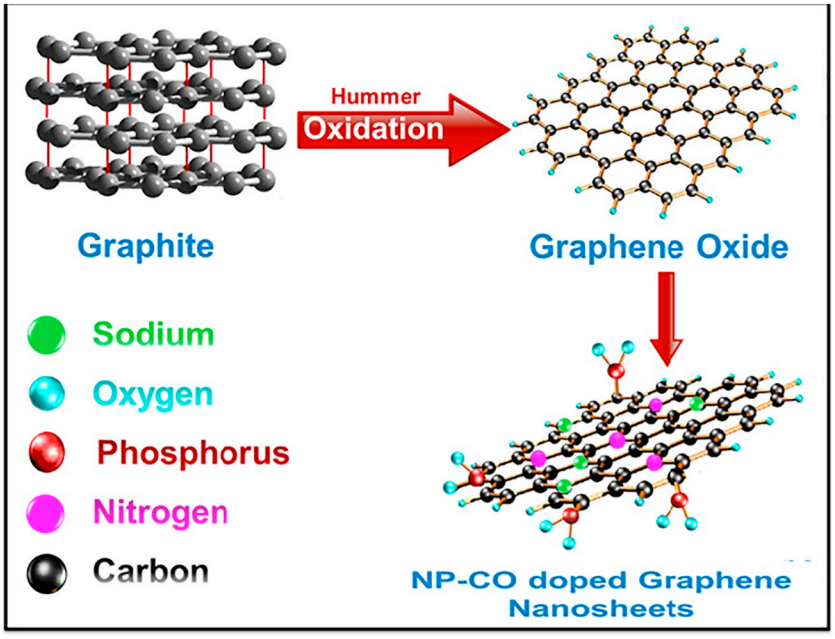


**Scheme 1.** Synthesis of functionalized and Na/N/P-co-doped graphene nanosheets with guanosine monophosphate disodium salt.

system: The working electrode was made from a glassy carbon disk 5.0 mm diameter, the standard calomel electrode (SCE) and platinum wire were used as a reference electrode and counter electrode, respectively. The electrochemical measurments were carried out in 0.5 M $H_2SO_4$ as aqueous media using Auto lab- 302 N electrochemical workstation (Metrohm), including cyclic voltammetry (CV) in the potential range from −0.2 to 1 V at various scan rates ranging from 1 to 200 mV/s, galvanostatic charge/discharge scan from −0.2 to 1 V at current density of at 0.1, 0.2, 0.4, 0.9, 1 and 2 A/g.

### 2.5. Characterization techniques

The crystal structure of the prepared materials was examined by X-ray diffractometer (XRD, XPERT-PRO-Analytical) with Cu Kα radiation (λ = 1.54°A). The surface morphology was investigated by field-emission scanning electron microscope (FESEM-Zeiss SEM Ultra-60) and high-resolution transmission electron microscope (HRTEM, JOEL JEM-2100) operating at an accelerating voltage of 120 kV. The infrared (IR) spectra were recorded using a JASCO spectrometer (FT/IR-6300 type A) in the range 400–4000 $cm^{-1}$. Raman measurements were performed using a micro-Raman microscope with an excitation laser beam wavelength of 325 nm. The thermal stability of the samples was examined using TGA thermal analyzer (TGA-Q500) from room temperature to 800 °C at a heating rate of 10 °C/min in nitrogen atmosphere."

## 3. Results and discussion

"Fig. 1 shows FESEM and TEM images of the fabricated materials. Fig. 1a depicts the surface morphology of the fabricated spongy graphene oxide (SGO), revealing a large increase in the thickness of graphene layers throughout the oxidization process due to the formation of oxygen groups in the basal plane of graphene [37]. Upon the addition of guanosine monophosphate disodium salts, the graphene became more exfoliated, resulting in well-defined corrugated and scrolled graphene sheets (Na/N/P-GNS), Fig. 1b. Those curls and wrinkles clearly act to prevent graphene sheets from restacking together with each other. Fig. 1c shows a TEM image of the fabricated SGO, which appeared crumpled with lots of folds. Fig. 1d depicts a TEM image of Na/N/P-GNS, showinga smooth and transparent surface with crumpled thin flake. These corrugations and wrinkles are most probably originated from the intercalated P defects in the Na/N/P-GNS.The surface wrinkling and folding also created bags of open edge sites, which are very promising sites for sensing and electrocatalytic applications [38]. The selected area electron diffraction pattern of the Na/N/P-GNS, Fig. 1e, shows a ring-like pattern with dispersed bright spots, suggesting that the P-doped graphene sheets became partially orientated, due to the structural distortion caused by the incorporation of P atoms into the graphitic planes."

"Fig. 2 illustrates the Raman spectra and the XRD pattern of pristine graphite, GO and Na/N/P-GNS. Fig. 2a shows the diffraction peak of graphite at 2θ = 26.5° corresponding to the diffraction from the (0 0 2) plane with an interlayer spacing of 0.34 nm. Upon chemical oxidation with $KMnO_4$, this diffraction peak was disappeared, indicating the complete oxidation of pristine graphite as evident by the single and sharp diffraction peak at 2θ = 12°, characteristic of GO with an interlayer spacing of 0.83 nm, suggesting that the GO is devoid of any graphite [39]. The spacing between the layer increases along the c-axis from 0.34 to 0.83 nm is owing to the existence of oxygen atoms on the GO sheets [40]. Upon functionalization of GO with guanosine monophosphate, the diffraction pattern shows a broad peak centered at 26° with the disappearance of the peak at 12°, indicating the restacking of graphene sheets and supports the formation of N/P-GNS with complete reduction of GO." Fig. 2b shows the Raman spectra of the fabricated SGO and Na/N/P-GNS. The spectrum of carbon nanomaterial is usually characterized by two main bands (D and G) ranging from 1200 to 1800 $cm^{-1}$. The intensity ratio of the D and G bands ($I_D/I_G$) is a useful parameter to determine the $sp^2$ domain size of a carbon structure containing $sp^3$ and $sp^2$ bonds. The spectra of SGO exhibited a G band at 1575.3 $cm^{-1}$ and a D band at 1359.6 $cm^{-1}$, with an $I_D/I_G$ ratio of 0.98. Upon functionalizing SGO with guanosine monophosphate, the G and D bands are shifted to 1582.2 and 1349 $cm^{-1}$, respectively and the D band becomes more prominent, resulting in a higher $I_D/I_G$ ratio (1.0). The higher $I_D/I_G$ ratio of N/P-GNS than that of GO suggest a higher disorder level due to the generation of smaller nano crystalline

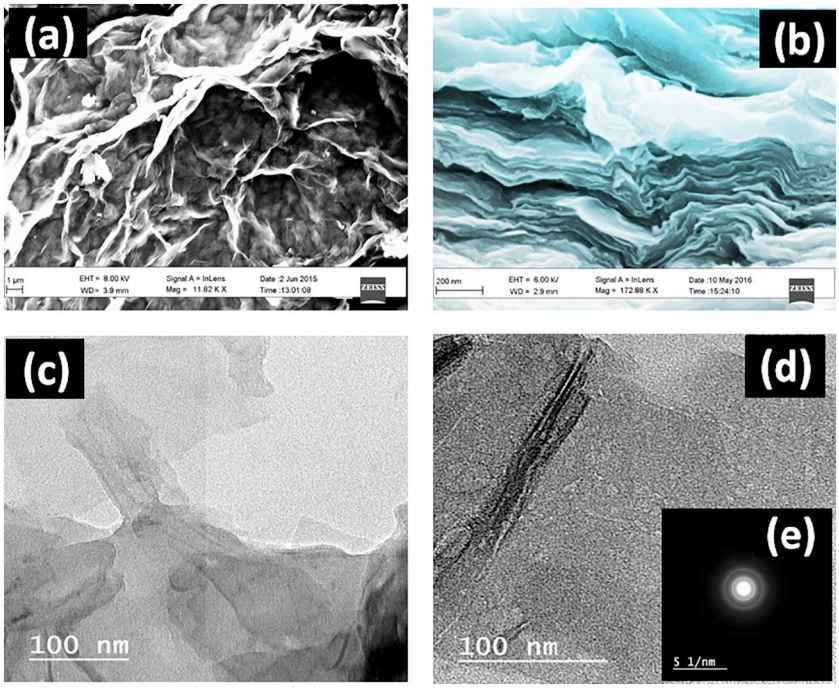


**Fig. 1.** FESEM images of (a) Spongy GO and (b) (N/P-GNS), and TEM images of (c) spongy GO, (d) (N/P-GNS), and (e) selected area electron diffraction pattern of N/P-doped GNS.

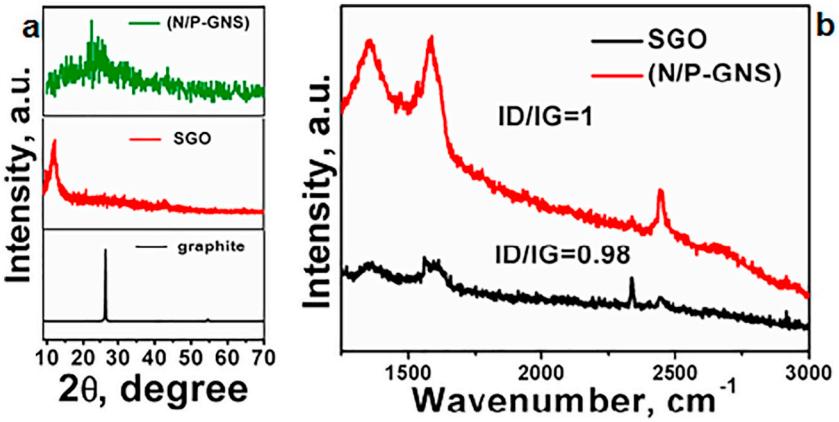


**Fig. 2.** (a) XRD pattern of pristine graphite, SGO and Na/N/P-GNS, and (b) Raman spectra of SGO and N/P-GNS.

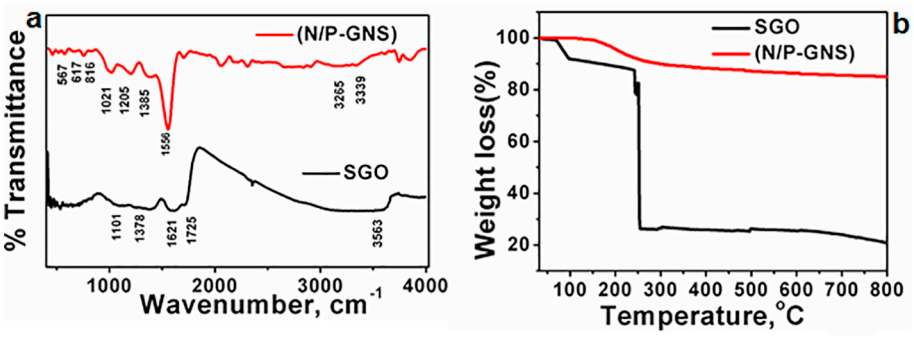


**Fig. 3.** (a) FTIR spectra and (b) TGA analysis of the fabricated SGO and Na/N/P-GNS.

graphene domains by heteroatom doping [41].

Fig. 3a shows the FTIR spectra of SGO and N/P-GNS. Graphene oxide is characterized as an insulator because of the physical damage of its conjugated structure, as a result of the action of strong acids. This process makes the graphene oxide layers in graphite oxide to be greatly oxygenated and attached with many carbonyl, carboxyl, and hydroxyl functional groups. The FTIR spectra of GO shows bands observed at 3563 $cm^{-1}$ 1725 $cm^{-1}$, 1621, 1378 $cm^{-1}$, and 1101 $cm^{-1}$, which can be assigned to O—H stretching vibrations $\nu$ ($OH_2$) ascribed to adsorbed water, the stretching vibrations $\nu$ (C = O) of COOH group corresponding to carbonyl and carboxyl groups, (C = C) from un-oxidized $sp^2$ CC bonds, O—H deformation of C–OH group, and $\nu$ (C—O) stretching vibrations mode [42]. On the other hand, the FTIR spectra of N/P-GNS indicates the disappearance of the peak at 1725 $cm^{-1}$ and the emergence of a new peak at 1556 $cm^{-1}$, which is a characteristic of the C═O stretching in the amide group, and a peak at 3339 $cm^{-1}$ characteristic of N—H stretching [43]. These peaks demonstrate that guanosine monophosphate molecules were covalently bonded to SGO by the amide linkage. Besides, some new bands observed at 1384 $cm^{-1}$, 1205 $cm^{-1}$, 1021 $cm^{-1}$, 3265 $cm^{-1}$, and 3339 $cm^{-1}$, which can be assigned to P═O, P-O-C, $NH_2$ and –OH [44], the vibrational modes (C═C twisting mode) of graphene at 816 $cm^{-1}$ and about 671 $cm^{-1}$ as well as the graphene skeletal vibrational mode at 567 $cm^{-1}$ [45].

"Fig. 3b shows the TGA results of the fabricated SGO and N/P-GNS upon heating under nitrogen atmosphere to 800 °C at a rate of 10 °C $min^{-1}$. The observed mass loss at temperatures below 100 °C is due to the removal of adsorbed water. The SGO material is thermally unstable and loses weight in three temperature zones; below 110 °C due to humidity content and vanishing of interstitial $H_2O$ [46] and the weight loss of mass was about 8%, around 130–250 °C due to the decomposition of hydroxyl groups, intercalated water and carboxyl groups to yield gasses as $H_2O$ and $CO_2$, where $CO_2$ [47], and from 350 to 800 °C with the highest loss reached about 80% can be ascribed to the decay of carbonyl group formed on the surface of graphene oxide to produce CO gas [48].Compared to the SGO, N/P-GNS showed higher thermal stability with no abrupt obvious mass loss till 200 °C. The material only exhibits mass loss of 14.5% at 800 °C, indicating that SGO is effectively reduced [49]. This is very beneficial for the use of the material in supercapacitors as it was shown before that the specific capacitance of reduced graphene oxide annealed at 200 °C was the highest and decreases with increasing the annealing temperature [50]. Moreover, the N/P-GNS preparation method in the present study avoids a high-temperature treatment to dope graphene with nitrogen and phosphorus compared to the previous reports [23–32,50]."

To confirm the Na/P/N co-doping, the elemental composition of N/P-GNS was investigated using X-ray photoelectron spectroscopy (XPS). Fig. 4a displays the XPS survey spectrum, showing a dominant C1s peak (~284.4 eV), an O1s peak (~532.0 eV), a P2p peak (~133.3 eV), an N1s peak (~399.9 eV), and a Na1s peak (~1071.3 eV), with resultant atomic percentages of 74.5, 13.6, 1.1, 5.4, and 5.5 at. %, respectively. Fig. 4b shows the C 1s high-resolution spectra, showing a singlet peak at 284.4 eV, which is attributed mainly to $sp^2$-hybridized graphitic carbon [51]. This singlet peak can be deconvoluted into four peaks: C1, C2, C3, and C4. The C1 peak located at a binding energy of 284.4 eV with a peak area proportion of 37.51% can be attributed to C—C bonding (sp2 carbon) in defect-free graphite lattice [52]. Peak C2 located at 284.9 eV with a peak area proportion of 14.24% is ascribed to carbon in the C—C bonding in defective graphite lattice and C—N $sp^2$ bonding [53]. The considerable presence of C2 demonstrates the defect structure and formation of an amide bond between the graphene and the guanosine monophosphate disodium salt. Peak C3 located at a bonding energy of 286.4 eV with a peak area proportion of 10.62% is attributed to carbon in C—O bonding [54]. Peak C4 located at 288.4 eV with a peak area proportion of 19.21% is attributed to carbon in a C═O amide bond [55]. To understand the nature of nitrogen species, the deconvolution of the N1s spectrum was performed as shown in Fig. 4c, where two

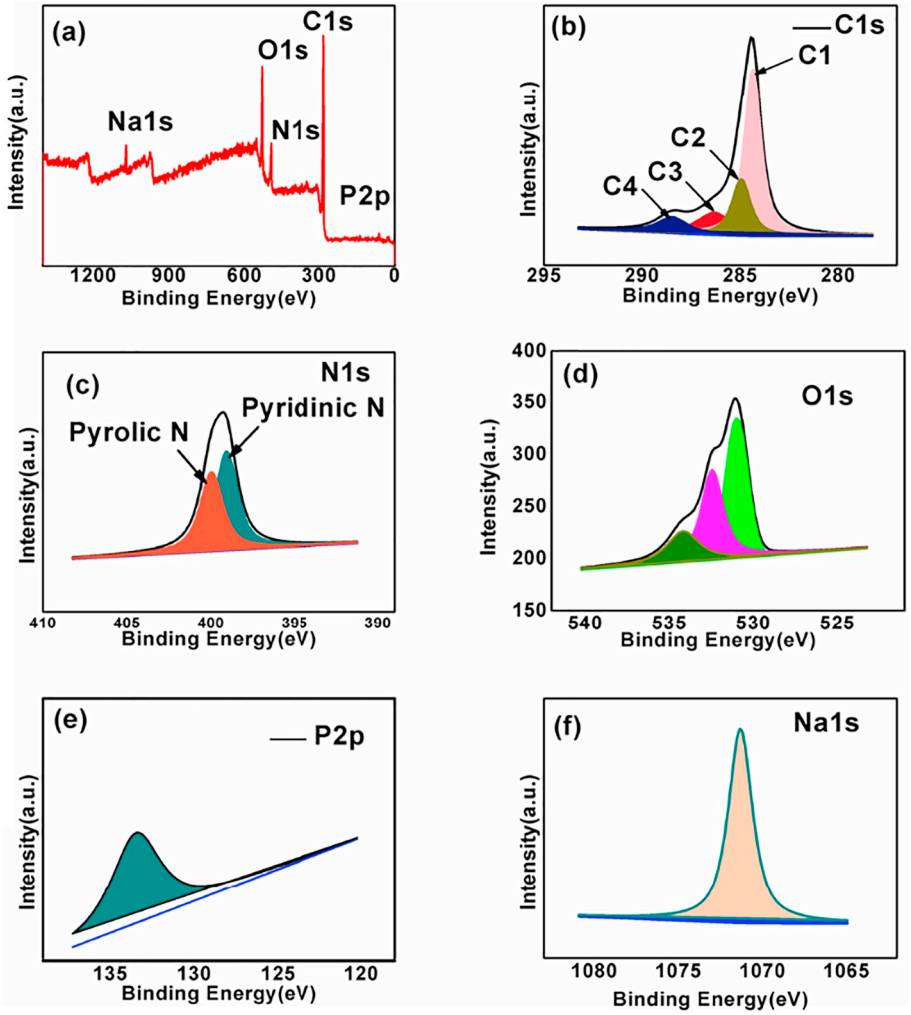


**Fig. 4.** X-ray photoelectron spectroscopy (XPS) analysis: (a) survey, and high resolution (b) C1s, (c) N1s, (d) O1s, (e) P2p, and (f) Na1s spectra of N/P-GNS.

peaks can be distinguished that can be ascribed to pyridine N at 399 eV and pyrrolic N at 400.01 eV [56]. The O1s peak can also be deconvoluted into three component peaks, Fig. 4d, where the peak at 530.9 eV may result from Na—O [57,58], the major peak at 532.5 eV can be assigned to the P—O bonding [59], and the peak at 534.1 eV can be ascribed to the C—O bonding [60]. The high-resolution P2p spectrum, Fig. 4e, indicates one type of chemical bonding as P—O at about 133.3 eV [61]. The deconvolution peaks of the Na1s spectrum were observed at 1071.3 eV, which may result from Na—O [62,63].

Cyclic voltammetry (CV) was performed to study the supercapacitive performance of the fabricated SGO and N/P-GNS samples in 0.5 M $H_2SO_4$. The specific capacitance of the electrode can be calculated from the CV curves using Eq. (1):

$$Cs = \frac{\int Idv}{vm\Delta V} \quad (1)$$

where *Cs* is the specific capacitance of the electrode (F/g), *m* is the mass of the active material (g), *I* is the response current density (A/g), $\Delta V$ is the potential difference (V) and *v* is the potential scan rate (mV/s). Fig. 5a shows the cyclic voltammograms of the SGO and N/P-GNS electrodes in 0.5 M $H_2SO_4$ at a scan rate of 1 mV/s. While the GO electrode shows insignificant current response due to its insulating physical characteristics, the current of the N/P-GNS electrode increases as the potential increases, suggesting an increasing electrical conductivity. The CV curves of the N/P-GNS electrode shows a rectangular shape at low scan rates, typical of electric double layer capacitive behavior [64], with a small deviation from the rectangular shape at 100 mV/s, in accordance with previous reports for graphene [65]. Irrespective of the scan rate, the N/P-GNS electrode shows a cathodic (reduction) peak at ~0.5 $V_{SCE}$ and a corresponding anodic peak at ~0.32 $V_{SCE}$, Fig. 5b. The specific capacitance of the N/P-GNS electrode reached 499 F/g at a scan rate of 1 mV/s and drops to 81.4 F/g at a scan rate of 200 mV/s, Fig. 5c. This is a common phenomenon as the ions in the electrolyte might not have enough time to move into the complex micropores of the electrodes (diffusion limited) at high scan speeds. Note that the obtained specific capacitance of 499 F/g at a scan rate of 1 mV/s is much higher than those previously reported for P, N co-doped graphene synthesized via a microwave-assisted method in the presence of ammonium polyphosphate (286 F/g in 1 M $H_2SO_4$) [66], and P, N co-doped carbon material (PNDC) produced from aminated tannin and poly phosphoric acid through microwave (161 F/g in 6 M KOH) [67], see Table 1. The obtained high specific capacitance of the fabricated N/P-GNS electrodes can be related to the synergistic effect of both N and P doping that could prompt Faradic reactions. Additionally, graphene became more exfoliated upon doping, facilitating the transportation of ions into the complex.

The measurements of galvanostatic charge/discharge at different current densities are performed in order to examine the suitability of the fabricated N/P-GNS electrodes for supercapacitor application. The charge/discharge curves have a quasi-triangular-shape with no noticeable IR drop observed. The specific capacitance was also calculated from the discharge curves at different current densities using Eq. (2):

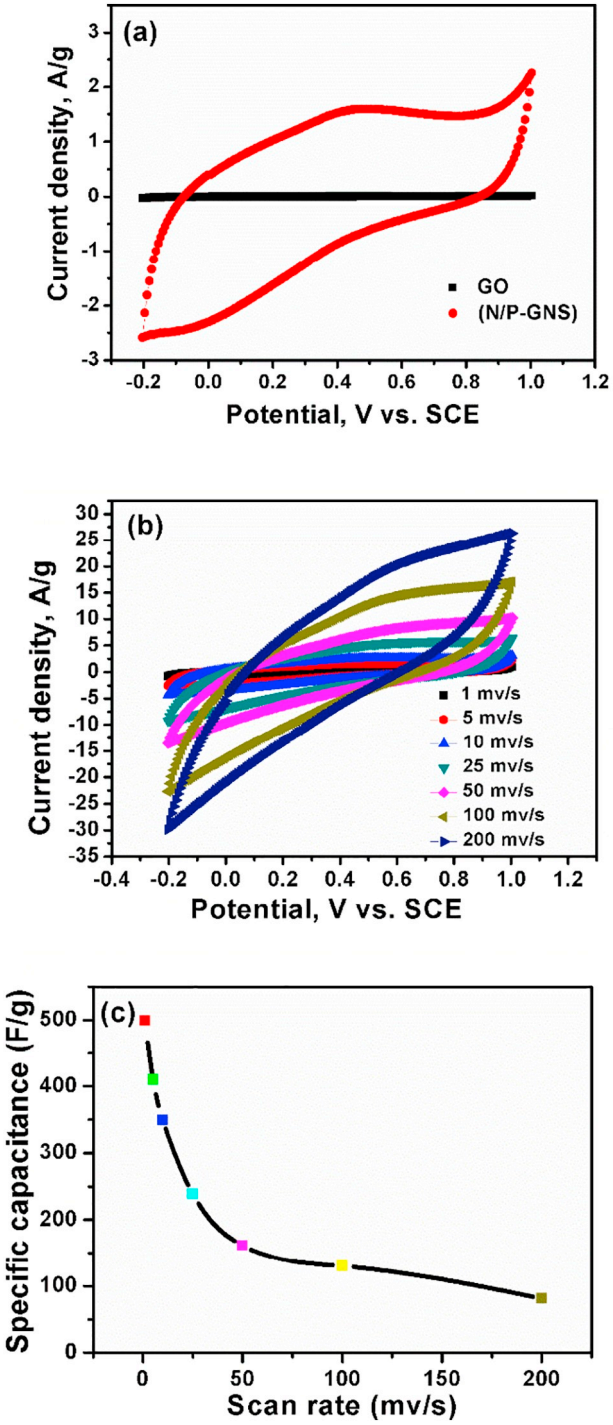


**Fig. 5.** (a) Cyclic voltammograms of N/P-GNS and GO electrodes at a scan rate of 5 mV/s, (b) cyclic voltammograms of N/P-GNS electrodes at different scan rates, and (c) the corresponding specific capacitance of N/P-GNS electrodes at different scan rates in 0.5 M $H_2SO_4$.

$$Cs = \frac{I\,\Delta t}{m\,\Delta V} \tag{2}$$

where I is the discharge current (A), Δt is the discharge time (s), and ΔV is the potential window (V). All the charge/discharge curves (Fig. 6a,b) are quasi-triangular, which may indicate fast and capable charge transfer as well as high electrical conductivity. The calculated specific capacitances are 492.9, 447.7, 429.9, 350.6, 344.8 and 291.6 F/g at 0.1, 0.2, 0.4, 0.9, 1 and 2 A/g, respectively. It was observed that 59.1% of the capacitance could be retained upon increasing the current density 20 times, indicating a good rate capability. The capacitance of the N/P-GNS is higher than those previously reported for N-doped graphene prepared via supercritical fluid-assisted processing in the presence of oxime (286 F/g in 1 M $H_2SO_4$ at a current density of 0.5 A/g) [68], in the presence of *o*-phenylenediamine (301 F/g in 6 M KOH at 0.1 A $g^{-1}$) [69], N-doped graphene aerogels functionalized with melamine (170.5 $Fg^{-1}$ at 0.2 $Ag^{-1}$ in 6 M KOH) [70], porous N-doped graphene/carbon nanotubes composite (PNGC) prepared by pyrolysis (246.6 $Fg^{-1}$ at a current density of 0.5 A $g^{-1}$ in 6 M of KOH) [71], N-doped graphene nano sheets prepared by one step supercritical fluid-assisted reaction of N-containing organic compounds with graphene oxide (280 F/g at a current density of 0.5 A $g^{-1}$ in 1 M $H_2SO_4$) [72], N,P,S-co doped Hierarchically Porous Carbon Spheres fabricated using the silica colloids, polyaniline, phytic acid and ammonium persulfate (274.5 $Fg^{-1}$ at 0.5 $Ag^{-1}$ in 6 M KOH) and N-rich porous carbons (417.5 F $g^{-1}$ at 0.5 A $g^{-1}$ in 6 M KOH) [73,74]. The obtained high specific capacitance of N/P-GNS electrode can be related to the co-doping effect that prevents the stacking of graphene layers and increases the electronegativity [73]. This co-doping may cause charge delocalization and the dipoles can draw charged species inside the surface of graphene producing Faradic redox reactions [75]. The positive effect of $Na^+$ can be related to the creation of p-type conductivity that improves capacitance and electrochemical activity of graphene by increasing the supported fast redox reactions [76,77].

The cycle life test of the fabricated N/P-GNS electrodes was performed at a scan rate of 200 mV/s for 1000 cycles, Fig. 6c. Note that the specific capacitance sharply increased from the initial cycle until 1000 cycle to be 101% of the initial cycle, indicating the excellent cycling stability of the fabricated N/P-GNS electrodes, which can be related to the increase of the electrolyte temperature during continuous operation over time. The energy and power densities are very important performance parameters of the supercapacitor, which can be calculated from the galvanostatic charge/discharge curves using Eqs. (3) and (4):

$$E = \frac{1}{2}Cs(\Delta V)^2 = \frac{I\Delta Vt}{2m} \tag{3}$$

$$P = \frac{E}{t} = \frac{I\Delta V}{m} \tag{4}$$

where *E* indicates the average energy density (Wh/kg), *P* is the average power density (W/kg), and *Cs* is the specific capacitance calculated from the charge/discharge curves. Ragone's plot of the N/P-GNS electrodes at different current densities is shown in Fig. 6d. The energy density can reach up to 98.58 Wh/kg with a power density of 59.99 W/kg at a current density of 0.1 A/g. Upon increasing the current density extremely to 2 A/g, the energy density remains at 58.3 Wh/kg with a reasonable power density of 1200 W/kg. note that the obtained energy density (98.58 Wh/kg) is much higher than those reported for un doped reduced graphene oxide (E = 11.6 Wh/kg and P = 250 W/kg) [78], RGO electrodes (E = 5.8 Wh/kg at 0.1 A/g) [79], mesoporous graphitic electrodes (E = 20 Wh/kg) [80], and N-doped graphene (NG) synthesized in the presence of hexamethylenetetramine flame with graphite oxide (E = 5.5 Wh/kg) [81].

## 4. Conclusion

Functionalize graphene (Na/N/P-GNS) was prepared via one-pot, green method. The electron microscopy (FESEM and TEM) analyses should the formation of crumpled exfoliated structure with lots of folds, which was attributed to the presence of guanosine monophosphate disodium salt between layers after covalent functionalization. This was confirmed by the XRD analysis, showing a broad diffraction peak centered at 26° with the disappearance of the peak at 12°, indicating the functionalization of SGO with the complete reduction of SGO. This was further confirmed via FTIR analysis, which showed a peak at 1556 $cm^{-1}$, characteristic of the C=O stretching in the amide group,

**Table 1**
Specific capacitances reported for co-doped graphene compared to our work.

| Material | Synthetic approach | Specific capacitance ($Fg^{-1}$) | Ref. |
|---|---|---|---|
| P,N co-doped graphene with ammonium polyphosphate | Microwave processing | (286 $Fg^{-1}$ in 1 M $H_2SO_4$) | [66] |
| P, N co-doped carbon material (PNDC) produced from aminated tannin and poly phosphoric acid | Microwave processing | (161 $Fg^{-1}$ in 6 M KOH) | [67] |
| N-doped graphene in the presence of oxime | Supercritical fluid-assisted processing | (286 $Fg^{-1}$ in 1 M $H_2SO_4$) | [68] |
| In the presence of *o*-phenylenediamine | | (301 $Fg^{-1}$ in 6 M KOH) | [69] |
| N-doped graphene aerogels functionalized with melamine | Annealing process at high temperatures | (170.5 $Fg^{-1}$ in 6 M KOH) | [70] |
| Porous N-doped graphene/carbon nanotubes composite (PNGC) | Pyrolysis processing | (246.6 $Fg^{-1}$ in 6 M of KOH) | [71] |
| N-doped graphene nano sheets | Supercritical fluid-assisted processing | (280 $Fg^{-1}$ in 1 M $H_2SO_4$) | [72] |
| N,P,S-co doped hierarchically porous carbon spheres | Polymerization reaction | (274.5 $Fg^{-1}$ at in 6 M KOH) | [73] |
| N-rich porous carbons | Carbonization processing | (417.5 $Fg^{-1}$ in 6 M KOH) | [74] |
| Functionalized Na/N/P co-doped graphene | Green, single-pot synthesis | (499 $Fg^{-1}$ in 0.5 M $H_2SO_4$) | Current work |

and a peak at 3339 $cm^{-1}$ characteristic of N—H stretching, confirming the covalent functionalization through the amide linkage. Also, bands appear at 1384 $cm^{-1}$, 1205 $cm^{-1}$, 1021 $cm^{-1}$, 3265 $cm^{-1}$ and 3339 $cm^{-1}$, which can be assigned to P═O, P-O-C, $NH_2$, and –OH. The Ramen spectra of N/P-GNS showed higher $I_D/I_G$ ratio (1.0) than that of SGO (0.98), indicating the introduction of $sp^3$ domain upon functionalization of SGO with guanosine mono phosphate disodium salt. The TGA analysis showed a slight weight loss of (14.5%) at 800 °C for the N/P-GNS electrode, indicating that the oxygen-based groups in GO have formed heat-stable structures due to the covalent bonding with guanosine monophosphate disodium salt. The XPS survey spectrum showed a dominant C 1s peak (~284.4 eV), an O 1 s peak (~532.0 eV), a P 2p peak (~133.3 eV), an N 1s peak (~399.9 eV), and a Na 1 s peak (~1071.3 eV) with resultant atomic percentages of 74.5, 13.6, 1.1, 5.4, and 5.5 at.%, respectively. The synthesized materials have been tested as supercapacitor electrodes in 0.5 M $H_2SO_4$ using cyclic voltammetry (CV) at different potential scan rates, and galvanostatic charge/discharge tests at different current densities. The N/P-GNS electrodes

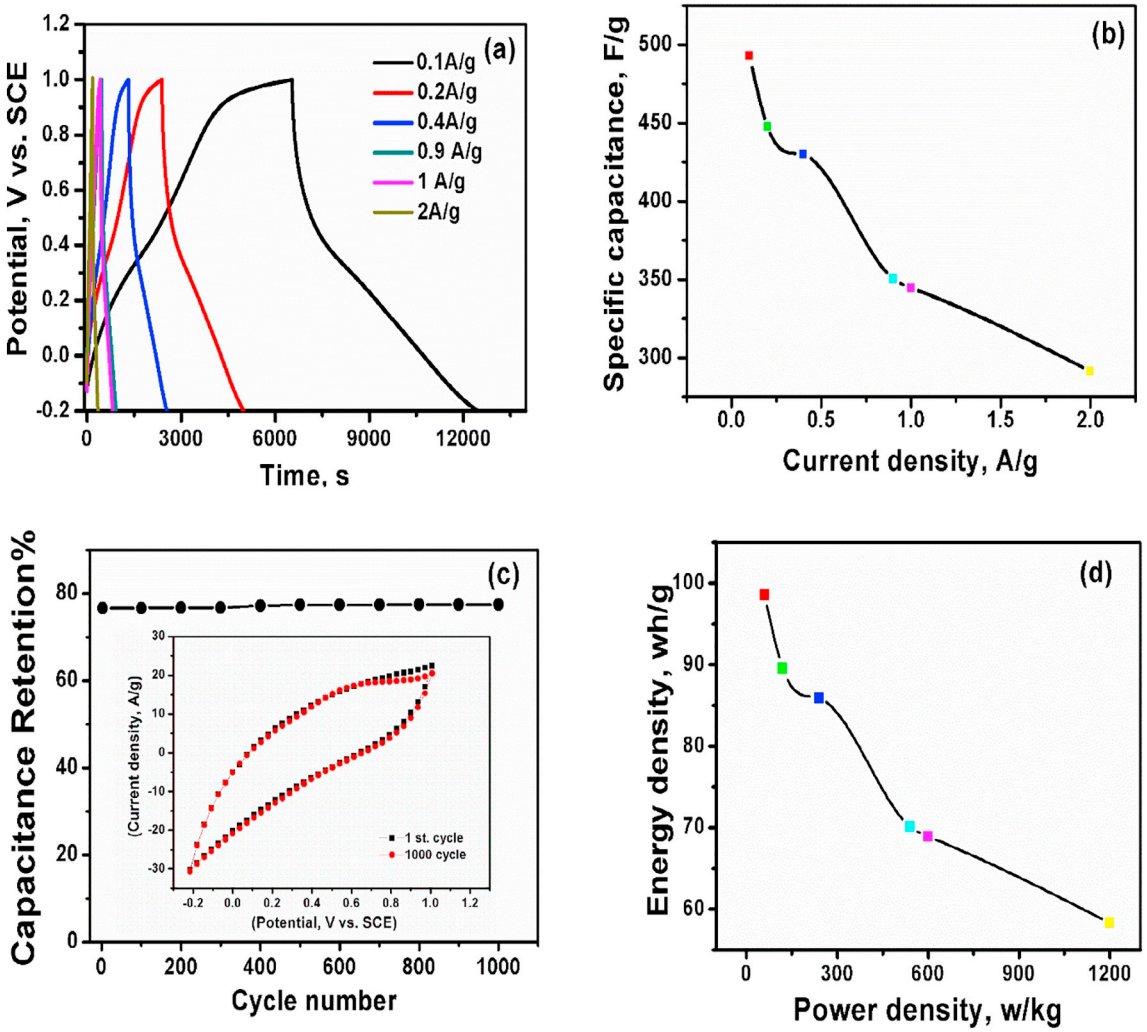


**Fig. 6.** (a) Galvanostatic charge/discharge curves of (N/P-GNS) electrode at different current densities. (b) Variation of specific capacitance against current density (c) CV curves of (N/P-GNS)electrode at the first and 1000th CV cycles of the. (d) Ragone plot related energy and power density at different current densities 1, 2, 3, 4 and 5 A/gin 0.5 M $H_2SO_4$.

showed a maximum specific capacitance of 499 F/g at a scan rate of 1 mV/s and exhibited excellent cycling retention of 101% after 1000 cycles at 200 mV/s. The energy density can reach up to 98.58 Wh/kg with a power density of 59.99 W/kg at a current density of 0.1 A/g. Those figures of merit are much greater than those reported for graphene-based materials examined under similar conditions. The observed high performance can be related to the synergistic effects of the spongy structure and the Na/N/P co-doping.

## Acknowledgment

The financial support of the present work by the American University in Cairo and the National Research Centre is highly appreciated.

## References

[1] M. Ramadan, A.M. Abdellah, S.G. Mohamed, N.K. Allam, 3D interconnected binder-free electrospun MnO@C nanofibers for supercapacitor devices, Sci. Rep. 8 (2018) 7988.
[2] A.E. Elkholy, F.E. Heakal, N.K. Allam, Nanostructured spinel manganese cobalt ferrite for high-performance supercapacitors, RSC Adv. 7 (2017) 51888–51895, https://doi.org/10.1039/C7RA11020K.
[3] A.E. Elkholy, F.E. Heakal, N.K. Allam, A facile electrosynthesis approach of amorphous Mn-Co-Fe ternary hydroxides as binder-free active electrode materials for high performance supercapacitors, Electrochim. Acta 296 (2019) 59–68, https://doi.org/10.1016/j.electacta.2018.11.038.
[4] H. Wang, H. Peng, G. Li, K. Chen, Nitrogen-containing carbon/graphene composite nanosheets with excellent lithium storage performances, Chem. Eng. J. 275 (2015) 160–167.
[5] F.M. Ismail, M. Ramadan, A.M. Abdellah, I. Ismail, N.K. Allam, Mesoporous spinel manganese zinc ferrite for high-performance supercapacitors, J. Electroanal. Chem. 817 (2018) 111–117, https://doi.org/10.1016/J.JELECHEM.2018.04.002.
[6] R. Mukkabla, P. Meduri, M. Deepa, P. Ghosal, Durable Li-S batteries with nano-sulfur/graphite nanoplatelets composites, Chem. Eng. J. 303 (2016) 369–383.
[7] P. Liang, F. Wang, A.-H. Zhong, Controlled synthesis of ordered sandwich $CuCo_2O_4$/reduced graphene oxide composites via layer-by-layer heteroassembly for high-performance supercapacitors, Chem. Eng. J. 350 (2018) 627–636, https://doi.org/10.1016/j.cej.2018.06.021.
[8] G. Yu, L. Hu, M. Vosgueritchian, H. Wang, X. Xie, J.R. McDonough, X. Cui, Y. Cui, Z. Bao, Solution-processed graphene/$MnO_2$ nanostructured textiles for high-performance electrochemical capacitors, Nano Lett. 11 (2011) 2905–2911, https://doi.org/10.1021/nl2013828.
[9] J.-S. Ye, H. Cui, X. Liu, T. Lim, W.-D. Zhang, F.-S. Sheu, Preparation and characterization of aligned carbon nanotube-ruthenium oxide nanocomposites for supercapacitors, Small 1 (2005) 560–565, https://doi.org/10.1002/smll.200400137.
[10] C. Guan, J. Liu, Y. Wang, L. Mao, Z. Fan, Z. Shen, H. Zhang, J. Wang, Iron oxide-decorated carbon for supercapacitor anodes with ultrahigh energy density and outstanding cycling stability, ACS Nano 9 (2015) 5198–5207, https://doi.org/10.1021/acsnano.5b00582.
[11] S.G. Mohamed, S.Y. Attia, N.K. Allam, One-step, calcination-free synthesis of zinc cobaltite nanospheres for high-performance supercapacitors, Mater. Today Energy 4 (2017) 97–104.
[12] T. Kim, G. Jung, S. Yoo, K.S. Suh, R.S. Ruoff, Activated graphene-based carbons as supercapacitor electrodes with macro- and mesopores, ACS Nano 7 (2013) 6899–6905, https://doi.org/10.1021/nn402077v.
[13] M.M. Hasan, N.K. Allam, Unbiased spontaneous solar hydrogen production using stable TiO2–CuO composite nanofiber photocatalysts, RSC Advances 8 (2018) 37219–37228.
[14] Y. Wang, M. Jaiswal, M. Lin, S. Saha, B. Özyilmaz, K.P. Loh, Electronic properties of nanodiamond decorated graphene, ACS Nano 6 (2012) 1018–1025, https://doi.org/10.1021/nn204362p.
[15] L. Ren, K.-N. Hui, K.S. Hui, Y. Liu, X. Qi, J. Zhong, Y. Du, J. Yang, 3D hierarchical porous graphene aerogel with tunable meso-pores on graphene nanosheets for high performance energy storage, Sci. Rep. 5 (2015) 14229, https://doi.org/10.1038/srep14229.
[16] A.S. Hassanien, R.A. Shedeed, N.K. Allam, Graphene quantum sheets with multi-band emission: unravelling the molecular origin of graphene quantum dots, J. Phys. Chem. C 120 (2016) 21678–21684.
[17] S. Pei, H.-M. Cheng, The reduction of graphene oxide, Carbon 50 (2012) 3210–3228, https://doi.org/10.1016/j.carbon.2011.11.010.
[18] J. Zhang, H. Yang, G. Shen, P. Cheng, J. Zhang, S. Guo, Reduction of graphene oxide via L-ascorbic acid, Chem. Commun. 46 (2010) 1112–1114, https://doi.org/10.1039/B917705A.
[19] Z. Zhang, X. Liu, X. Qi, Z. Huang, L. Ren, J. Zhong, Hydrothermal synthesis of $Ni_3S_2$/graphene electrode and its application in a supercapacitor, RSC Adv. 4 (2014) 37278–37283, https://doi.org/10.1039/C4RA05078A.
[20] X. Liua, X. Qia, Z. Zhang, L. Rena, Y. Liua, L. Menga, K. Huanga, J.Z. Wang, M. Zhi, J. Wu, X. Zhang, One-step electrochemical deposition of nickel sulfide/graphene and its use for supercapacitors, Ceram. Int. 40 (2014) 8189–8193.
[21] X.-Y. Zhang, S.-H. Sun, X.-J. Sun, Y.-R. Zhao, L. Chen, Y. Yang, W. Lü, D.-B. Li, Plasma-induced, nitrogen-doped graphene-based aerogels for high-performance supercapacitors, Light. Sci. Appl. 5 (2016) e16130, https://doi.org/10.1038/lsa.2016.130.
[22] L. Qu, Y. Liu, J.-B. Baek, L. Dai, Nitrogen-doped graphene as efficient metal-free electrocatalyst for oxygen reduction in fuel cells, ACS Nano 4 (2010) 1321–1326, https://doi.org/10.1021/nn901850u.
[23] M. Aliofkhazraei, N. Ali, W.I. Milne, C.S. Ozkan, S. Mitura, J.L. Gervasoni, Graphene Science Handbook: Mechanical and Chemical Properties, CRC Press, 2016.
[24] R. Canty, E. Gonzalez, C. MacDonald, S. Osswald, H. Zea, C.C. Luhrs, Reduction Expansion Synthesis as Strategy to Control Nitrogen Doping Level and Surface Area in Graphene, Materials 8 (2015) 7048–7058, https://doi.org/10.3390/ma8105359.
[25] X. Wang, X. Li, L. Zhang, Y. Yoon, P.K. Weber, H. Wang, J. Guo, H. Dai, N-doping of graphene through electrothermal reactions with ammonia, Science 324 (80) (2009) 768–771, https://doi.org/10.1126/science.1170335.
[26] D. Geng, Y. Chen, Y. Chen, Y. Li, R. Li, X. Sun, S. Ye, S. Knights, High oxygen-reduction activity and durability of nitrogen-doped graphene, Energy Environ. Sci. 4 (2011) 760, https://doi.org/10.1039/c0ee00326c.
[27] J. Shah, J. Lopez-Mercado, M.G. Carreon, A. Lopez-Miranda, M.L. Carreon, Plasma Synthesis of Graphene from Mango Peel, ACS Omega 3 (1) (2018) 455–463.
[28] W. Qian, X. Cui, R. Hao, Y. Hou, Z. Zhang, Facile preparation of nitrogen-doped few-layer graphene via supercritical reaction, ACS Appl. Mater. Interfaces 3 (2011) 2259–2264, https://doi.org/10.1021/am200479d.
[29] Z.-W. Liu, F. Peng, H.-J. Wang, H. Yu, W.-X. Zheng, J. Yang, Phosphorus-doped graphite layers with high electrocatalytic activity for the $O_2$ reduction in an alkaline medium, Angew. Chem. Int. Ed. 50 (2011) 3257–3261, https://doi.org/10.1002/anie.201006768.
[30] R. Li, Z. Wei, X. Gou, W. Xu, Phosphorus-doped graphene nanosheets as efficient metal-free oxygen reduction electrocatalysts, RSC Adv. 3 (2013) 9978, https://doi.org/10.1039/c3ra41079j.
[31] S. Dey, A. Govindaraj, K. Biswas, C.N.R. Rao, Luminescence properties of boron and nitrogen doped graphene quantum dots prepared from arc-discharge-generated doped graphene samples, Chem. Phys. Lett. 595–596 (2014) 203–208, https://doi.org/10.1016/j.cplett.2014.02.012.
[32] Z. Wen, S. Ci, F. Zhang, X. Feng, S. Cui, S. Mao, S. Luo, Z. He, J. Chen, Nitrogen-enriched core-shell structured Fe/$Fe_3C$-C nanorods as advanced electrocatalysts for oxygen reduction reaction, Adv. Mater. 24 (2012) 1399–1404, https://doi.org/10.1002/adma.201104392.
[33] S. Yang, X. Feng, X. Wang, K. Müllen, Graphene-based carbon nitride nanosheets as efficient metal-free electrocatalysts for oxygen reduction reactions, Angew. Chem. Int. Ed. 50 (2011) 5339–5343, https://doi.org/10.1002/anie.201100170.
[34] C.N.R. Rao, A.K. Sood, K.S. Subrahmanyam, A. Govindaraj, Graphene: the new two-dimensional nanomaterial, Angew. Chem. Int. Ed. 48 (2009) 7752–7777, https://doi.org/10.1002/anie.200901678.
[35] D.M. El-Gendy, N.A.A. Ghany, E.E.F. El Sherbini, N.K. Allam, Adenine-functionalized spongy graphene for green and high-performance supercapacitors, Sci. Rep. 7 (2017) 43104, https://doi.org/10.1038/srep43104.
[36] M.A. Mohamed, D.M. El-Gendy, N. Ahmed, C.E. Banks, N.K. Allam, 3D spongy graphene-modified screen-printed sensors for the voltammetric determination of the narcotic drug codeine, Biosens. Bioelectron. 101 (2018) 90–95, https://doi.org/10.1016/j.bios.2017.10.020.
[37] D.R. Dreyer, S. Park, C.W. Bielawski, R.S. Ruoff, The chemistry of graphene oxide, Chem. Soc. Rev. 39 (2010) 228–240, https://doi.org/10.1039/b917103g.
[38] Y. He, W. Chen, C. Gao, J. Zhou, X. Li, E. Xie, An overview of carbon materials for flexible electrochemical capacitors, Nanoscale 5 (2013) 8799, https://doi.org/10.1039/c3nr02157b.
[39] D. Long, W. Li, L. Ling, J. Miyawaki, I. Mochida, S.-H. Yoon, Preparation of nitrogen-doped graphene sheets by a combined chemical and hydrothermal reduction of graphene oxide, Langmuir 26 (2010) 16096–16102, https://doi.org/10.1021/la102425a.
[40] F. Liu, J. Sun, L. Zhu, X. Meng, C. Qi, F.-S. Xiao, Sulfated graphene as an efficient solid catalyst for acid-catalyzed liquid reactions, J. Mater. Chem. 22 (2012) 5495, https://doi.org/10.1039/c2jm16608a.
[41] M.M. Hasan, S.A. Tolba, N.K. Allam, In situ formation of graphene stabilizes zero-valent copper nanoparticles and significantly enhances the efficiency of photo-catalytic water splitting, ACS Sustain. Chem. Eng. 6 (2018) 16876–16885.
[42] Y. Xu, Y. Wang, J. Liang, Y. Huang, Y. Ma, X. Wan, Y. Chen, A hybrid material of graphene and poly (3,4-ethyldioxythiophene) with high conductivity, flexibility, and transparency, Nano Res. 2 (2009) 343–348, https://doi.org/10.1007/s12274-009-9032-9.
[43] G. Socrates, Infrared and Raman Characteristic Group Frequencies: Tables and Charts, John Wiley & Sons, 2004.
[44] C.D. Zangmeister, Preparation and evaluation of graphite oxide reduced at 220 °C, Chem. Mater. 22 (2010) 5625–5629, https://doi.org/10.1021/cm102005m.
[45] Z. Lei, L. Lu, X.S. Zhao, The electrocapacitive properties of graphene oxide reduced by urea, Energy Environ. Sci. 5 (2012) 6391–6399, https://doi.org/10.1039/C1EE02478G.
[46] Y. Tao, X. Xie, W. Lv, D.-M. Tang, D. Kong, Z. Huang, H. Nishihara, T. Ishii, B. Li, D. Golberg, F. Kang, T. Kyotani, Q.-H. Yang, Towards ultrahigh volumetric capacitance: graphene derived highly dense but porous carbons for supercapacitors, Sci. Rep. 3 (2013) 2975, https://doi.org/10.1038/srep02975.
[47] M. Lee, B.-H. Wee, J.-D. Hong, High performance flexible supercapacitor electrodes composed of ultralarge graphene sheets and vanadium dioxide, Adv. Energy Mater. 5 (2015) 1401890, https://doi.org/10.1002/aenm.201401890.
[48] Z.-H. Sheng, L. Shao, J.-J. Chen, W.-J. Bao, F.-B. Wang, X.-H. Xia, Catalyst-free synthesis of nitrogen-doped graphene via thermal annealing graphite oxide with

melamine and its excellent electrocatalysis, ACS Nano 5 (2011) 4350–4358, https://doi.org/10.1021/nn103584t.
[49] C.H. Choi, S.H. Park, S.I. Woo, Heteroatom doped carbons prepared by the pyrolysis of bio-derived amino acids as highly active catalysts for oxygen electro-reduction reactions, Green Chem. 13 (2011) 406–412, https://doi.org/10.1039/C0GC00384K.
[50] A.M. Puziy, O.I. Poddubnaya, R.P. Socha, J. Gurgul, M. Wisniewski, XPS and NMR studies of phosphoric acid activated carbons, Carbon 46 (2008) 2113–2123, https://doi.org/10.1016/j.carbon.2008.09.010.
[51] L.S. Panchakarla, K.S. Subrahmanyam, S.K. Saha, A. Govindaraj, H.R. Krishnamurthy, U.V. Waghmare, C.N.R. Rao, Synthesis, Structure and Properties of Boron and Nitrogen Doped Graphene, 21 (2009), pp. 4726–4730, https://doi.org/10.1002/adma.200901285.
[52] D. Wei, Y. Liu, H. Zhang, L. Huang, B. Wu, J. Chen, G. Yu, Scalable synthesis of few-layer graphene ribbons with controlled morphologies by a template method and their applications in nanoelectromechanical switches, J. Am. Chem. Soc. 131 (2009) 11147–11154, https://doi.org/10.1021/ja903092k.
[53] W. Zhang, J. Cui, C. Tao, Y. Wu, Z. Li, L. Ma, Y. Wen, G. Li, A strategy for producing pure single-layer graphene sheets based on a confined self-assembly approach, Angew. Chem. Int. Ed. 48 (2009) 5864–5868, https://doi.org/10.1002/anie.200902365.
[54] B.A. Ali, O.I. Metwalli, A.S.G. Khalil, N.K. Allam, Unveiling the effect of the structure of carbon material on the charge storage mechanism in $MoS_2$-based supercapacitors, ACS Omega 3 (2018) 16301–16308, https://doi.org/10.1021/acsomega.8b02261.
[55] N. Daems, X. Sheng, I.F.J. Vankelecom, P.P. Pescarmona, Metal-free doped carbon materials as electrocatalysts for the oxygen reduction reaction, J. Mater. Chem. A 2 (2014) 4085–4110, https://doi.org/10.1039/C3TA14043A.
[56] K. Xu, Electrolytes and interphases in Li-ion batteries and beyond, Chem. Rev. 114 (2014) 11503–11618, https://doi.org/10.1021/cr500003w.
[57] P. Ge, M. Fouletier, Electrochemical intercalation of sodium in graphite, Solid State Ionics 28–30 (1988) 1172–1175.
[58] Ha. Kima, J. Honga, G. Yoona, H. Kimc, K.-Y. Parka, M.-S. Parkd, W.-S. Yoonc, K. Kang, Sodium Intercalation Chemistry in Graphite, Energy Environ. Sci. 8 (2015) 2963–2969.
[59] N. Ahmed, M. Ramadan, W.M.A. El Rouby, A.A. Farghali, N.K. Allam, Non-precious co-catalysts boost the performance of TiO2 hierarchical hollow mesoporous spheres in solar fuel cells, Int. J. Hydrog. Energy 43 (2018) 21219–21230.
[60] S. Huang, Y. Meng, S. He, A. Goswami, Q. Wu, J. Li, S. Tong, T. Asefa, M. Wu, N-, O-, and S-tridoped carbon-encapsulated Co 9 S 8 nanomaterials: efficient bifunctional electrocatalysts for overall water splitting, Adv. Funct. Mater. 27 (2017) 1606585, https://doi.org/10.1002/adfm.201606585.
[61] Z. Hu, Z. Shen, J.C. Yu, Phosphorus containing materials for photocatalytic hydrogen evolution, Green Chem. 19 (2017) 588–613, https://doi.org/10.1039/C6GC02825J.
[62] M.L. Casais-Molina, C. Cab, G. Canto, J. Medina, A. Tapia, Carbon nanomaterials for breast cancer treatment, J. Nanomater. 2018 (2018), https://doi.org/10.1155/2018/2058613 (Mater. 2008, 18, 3506).
[63] Z. Lin, H. Tian, F. Xu, X. Yang, Y. Mai, X. Feng, Facile synthesis of bowl-shaped nitrogen-doped carbon hollow particles templated by block copolymer “kippah vesicles” for high performance supercapacitors, Polym. Chem. 7 (2016) 2092–2098, https://doi.org/10.1039/C6PY00161K.
[64] M. Seredych, T.J. Bandosz, S-doped micro/mesoporous carbon–graphene composites as efficient supercapacitors in alkaline media, J. Mater. Chem. A 1 (2013) 11717, https://doi.org/10.1039/c3ta12252b.
[65] S.K. Ramasahayam, A.L. Clark, Z. Hicks, T. Viswanathan, Spent coffee grounds derived P, N co-doped C as electrocatalyst for supercapacitor applications, Electrochim. Acta 168 (2015) 414–422, https://doi.org/10.1016/j.electacta.2015.03.193.
[66] B.S. Suresh, A. Elavarasan, M. Sathish, High performance supercapacitor using N-doped graphene prepared via supercritical fluid processing with an oxime nitrogen source, Electrochim. Acta 200 (2016) 37–45.
[67] Y. Lu, F. Zhang, T. Zhang, K. Leng, L. Zhang, X. Yang, Y. Ma, Y. Huang, M. Zhang, Y. Chen, Synthesis and supercapacitor performance studies of N-doped graphene materials using o-phenylenediamine as the double-N precursor, Carbon 63 (2013) 508–516, https://doi.org/10.1016/J.CARBON.2013.07.026.
[68] L.-B. Xing, S.-F. Hou, J. Zhou, J.-L. Zhang, W. Si, Y. Dong, S. Zhuo, Three dimensional nitrogen-doped graphene aerogels functionalized with melamine for multifunctional applications in supercapacitors and adsorption, J. Solid State Chem. 230 (2015) 224–232, https://doi.org/10.1016/j.jssc.2015.07.009.
[69] M. Wang, H. Zhang, C. Wang, X. Hu, G. Wang, Direct electrosynthesis of poly-o-phenylenediamine bulk materials for supercapacitor application, Electrochimica Acta 91 (2013) 144–151.
[70] D. Hulicova-Jurcakova, M. Seredych, G.Q. Lu, N.K.A.C. Kodiweera, P.E. Stallworth, S. Greenbaum, T.J. Bandosz, Effect of surface phosphorus functionalities of activated carbons containing oxygen and nitrogen on electrochemical capacitance, Carbon 47 (2009) 1576–1584, https://doi.org/10.1016/j.carbon.2009.02.006.
[71] T.-T. Lin, W.-H. Lai, Q.-F. Lü, Y. Yu, Porous nitrogen-doped graphene/carbon nanotubes composite with an enhanced supercapacitor performance, Electrochim. Acta 178 (2015) 517–524.
[72] M. Sathish, S. Mitani, T. Tomai, I. Honma, Supercritical fluid assisted synthesis of N-doped graphene nanosheets and their capacitance behavior in ionic liquid and aqueous electrolytes, J. Mater. Chem. A 20 (2014) 4731.
[73] L. Yan, D. Li, T. Yan, G. Chen, L. Shi, Z. An, D. Zhang, N,P,S-co doped hierarchically porous carbon spheres with well-balanced gravimetric/volumetric capacitance for supercapacitors, ACS Sustain. Chem. Eng. 64 (2018) 5265–5272.
[74] B. Chang, W. Shi, S. Han, Y. Zhou, Y. Liu, S. Zhang, B. Yang, N-rich porous carbons with a high graphitization degree and multiscale pore network for boosting high-rate supercapacitor with ultrafast charging, Chem. Eng. J. 18 (2008) S1385–S8947, https://doi.org/10.1016/j.cej.2018.06.013.
[75] Z. Zhang, L. Ren, W. Han, L. Meng, X. Wei, X. Qi, J. Zhong, One-pot electro deposition synthesis of ZnO/graphene composite and its use as binder-free electrode for supercapacitor, Ceram. Int. 11 (2014) S0272–S8842.
[76] Q. Ye, R. Dong, Z. Xia, G. Chen, H. Wang, G. Tan, L. Jiang, F. Wang, Enhancement effect of Na ions on capacitive behavior of amorphous $MnO_2$, Electrochim. Acta 141 (2014) 286–293.
[77] Y.X. Wang, Y.G. Lim, M.S. Park, S.L. Chou, J.H. Kim, H.K. Liu, S.X. Dou, Y.J. Kim, Ultrafine $SnO_2$ nanoparticle loading onto reduced graphene oxide as anodes for sodium-ion batteries with superior rate and cycling performances, J. Mater. Chem. 2 (2014) 529–534.
[78] J. Hu, Z. Kang, F. Li, X. Huang, Graphene with three-dimensional architecture for high performance supercapacitor, Carbon 67 (2014) 221–229.
[79] C.M. Chen, Q. Zhang, X.C. Zhao, B.S. Zhang, Q.Q. Kong, M.G. Yang, Q.H. Yang, M.Z. Wang, Y.G. Yang, R. Schlögl, D.S. Su, Hierarchically aminated graphene honeycombs for electrochemical capacitive energy storage, J. Mater. Chem. 22 (2012) 14076–14084.
[80] Y. Sun, Q. Wu, Y. Xu, H. Bai, C. Li, G. Shi, Highly conductive and flexible mesoporous graphitic films prepared by graphitizing the composites of graphene oxide and nanodiamond, J. Mater. Chem. 21 (2011) 7154, https://doi.org/10.1039/c0jm04434b.
[81] Y.-Z. Liu, Y.-F. Li, F.-Y. Su, L.-J. Xie, Q.-Q. Kong, X.-M. Li, J.-G. Gao, C.-M. Chen, Easy one-step synthesis of N-doped graphene for supercapacitors, Energy Storage Mater. 2 (2016) 69–75.